Appl Phys A
DOI 10.1007/s00339-011-6732-2

Applied Physics A
Materials Science & Processing

INVITED PAPER

Polarization-controlled spatial localization of near-field energy in planar symmetric coupled oligomers

M. Rahmani · B. Lukiyanchuk · T. Tahmasebi · Y. Lin · T.Y.F. Liew · M.H. Hong

Received: 12 July 2011 / Accepted: 8 December 2011

Abstract Arrays of planar symmetric coupled oligomers support higher sensitivity optical response than uncoupled plasmonic systems. In this work, the transition from isolated to collective optical modes in plasmonic oligomers, such as pentamers and quadrumers, is investigated via experimental characterization and simulation with good agreement. The designed and fabricated metallic oligomers consist of a single central disk and outer ring-like disks in nanoscales. It is shown that while the far-field spectral responses of oligomers are polarization-independent, due to the structure symmetry, the spatial localization of near-field energy in nanogaps can be polarization-controlled. This localization is established at a normal-incident light of a single source rather than co-illumination by two light sources accompanied by different incident angles or phase shift. It can overcome the spatial restrictions of conventional optics. The influence of the nano-disk sizes and gaps among them on the intensity and shape of the localized near-field energy in pentamers and quadrumers is also studied.

1 Introduction

The coupling between individual metallic nanoparticles supports collective electronic oscillations of the entire structure. This phenomenon, which is known as surface plasmon resonance, is a topic of intense contemporary interest [1]. Recent studies show that the energies transferring from an initial state to a final state of metallic nanostructures can interfere both constructively and destructively. This transition has been carried out from isolated to collective modes when the surrounding satellite nano-particles approach a unique central nano-particle [2].

The resulting relative phase of the plasmon oscillations in the individual nanoparticles of the complex can lead to the excitation of new sets of collective plasmon modes [3]. Well studied plasmon resonances of isolated nanostructures, such as disks, triangles, rods, and rings, are the good examples of plasmon constructive interferences, in which the spectral behavior can be tuned easily by varying the shape and size of nano-particles [1]. When the plasmons destructively interfere, the resulting collective plasmon modes can be excited at distinct energies that depend on the relative phase of the plasmon oscillations in the individual nanoparticles of the complex. It can lead to many novel phenomena, such as "hot-spots" [4] which are induced from resonant excitation based on the large electromagnetic field enhancement, as well as electromagnetically induced transparency (EIT) [4] and Fano Resonance (FR) [3]. While EIT is a quantum interference effect that reduces light absorption over a narrow spectral region in a coherently driven atomic system [5], the microscopic origin of the FR was introduced from the interference of a narrow discrete resonance with a broad spectral line or continuum [3, 6]. The characteristics of EIT and FR were firstly demonstrated in the mechanical systems of coupled oscillators [7]. Later, analogies between classical oscillators and surface plasmons led to the introduction of EIT and FRs at optical frequencies [8].

M. Rahmani · B. Lukiyanchuk · T. Tahmasebi · Y. Lin · T.Y.F. Liew · M.H. Hong
Data Storage Institute, (A*STAR) Agency for Science, Technology and Research, 5 Engineering Drive 1, Singapore 117608, Singapore

M. Rahmani · T. Tahmasebi · T.Y.F. Liew · M.H. Hong (✉)
Department of Electrical and Computer Engineering, National University of Singapore, 4 Engineering Drive 3, Singapore 117576, Singapore
e-mail: elehmh@nus.edu.sg
Fax: +65-67791103

Published online: 22 December 2011

FRs in nanoscale plasmonic systems have been obtained with symmetry breaking [9], breaking of time reversal symmetry [10], multiple metallic elements [11] or tuning of incidence angle [11]. These asymmetric conditions, which depend on polarization, allow high-order multipolar modes to be excited and coupled with directly excited dipolar modes leading to FR appearance. Recently, it has been demonstrated that FR can be arisen not only with the coupling of dipolar and multipolar modes but also the coupling of the anti-parallel dipolar modes as well in coupled plasmonic structures [2, 12–15]. Furthermore, the higher sensitivity optical response of these coupled structures as compared to the uncoupled ones have attracted interest in these symmetrical structures, such as heptamers [2, 12]. However, the low ratio of the anti-parallel to the parallel dipoles arising from the individual components in these coupled heptamers is attributed to relatively weak FR [13].

In this paper, arrays of plasmonic pentamers [13, 14] and quadrumers [15] consisting of central and surrounding metallic nano-disks of the same size were designed and fabricated. In order to explore the plasmon interactions among the disks on their optical properties, arrays of plasmon monomers and ring-like quadrumers were fabricated and characterized as well. In some of previous studies, the objective characteristics were established at $\sim 50^\circ$ angle of the incidence because of the retardation effect in the heptamer structures [12]. But in this paper, it was found that in relation to the previous studies of heptamers, reduction in the number of surrounding disks leads to an enhancement in the ratio of anti-parallel dipoles to the parallel dipoles. It generates a stronger FR, which is quite observable at a normal light incidence. Meanwhile, controlling light localization with nanoplasmonics is one of more promising areas which can make metallic nanostructures good candidates for various applications, such as sensing [16]. In this work, we have shown that the near-field energy distribution in the designed quadrumer and pentamer can be flexibly tuned by changing the excitation polarization, while the collective optical response, such as FR, are polarization-independent. This energy localization can be established at a normal-incident light of a single source rather than co-illumination by two light sources at different incident angles or phase shifts [17, 18]. It can overcome the spatial restriction of the conventional optics with unique potential applications in nano-lithography [19] and non-linear spectroscopy [18]. The effects of the disk size and the gap among the disks on the intensity and shape of this excited near-field energy "hot-spots" are studied as well.

2 Experimental

Arrays of monomers, ring-like quadrumers, quadrumers and pentamers, were fabricated by electron beam lithography (Elonix 100KV EBL system) on quartz substrates to investigate transmission responses. A 3 nm thick Ti film was first deposited by e-beam evaporation (EB03 BOC Edwards) on the substrates to increase the Au adhesion followed by 60 nm Au film. Subsequently Hydrogen Silse-Squioxane (HSQ) as a negative electro-resist (thickness: 50 nm) was spin coated. The samples were baked at $\sim 200^\circ$C for 120 seconds. After exposure and development, the nanostructures on the electro-resist were transferred down to the metallic films by ion milling. To characterize the fabricated samples, a UV-Vis-NIR micro-spectrophotometer (CRAIC QDI 2010 based on a Leica DMR microscope) was used. Normal-incident light with linear polarizations was applied to excite the structures. Simulated curves were obtained by a three-dimensional finite-difference time domain technique (FDTD) using a perfectly matched layer (PML) around the structures in the wavelength range of 300–1300 nm. The dielectric functions used for the simulation were obtained from the experimental data of Johnson and Christy [20].

3 Results and discussion

The nanostructures under consideration are illustrated in Fig. 1. In order to gain physical insight into the coupling among nano-disks, the monomer and ring-like quadrumer as the constituent components of the pentamer were also fabricated in the same sizes as those in the pentamer array. Figures 1(a)–(d) show the SEM images of the periodic patterns of monomers, ring-like quadrumers, pentamers and quadrumers, respectively. The diameter and height of disks are 142 nm and 60 nm, respectively, and the gap between the disks in the pentamers is 18 nm. Since the arisen plasmons are extremely sensitive to the shape of structures, significant efforts have been made to fabricate well shaped nano-disks with minimum size variation.

The optical responses of plasmonic monomers, ring-like quadrumers, quadrumers and pentamers were simulated as shown in Fig. 2(a). The measured transmission spectra of the structures fabricated on the quartz substrates are displayed in Fig. 2(b). Apart from a red shift due to the absence of substrate in the simulation, the measured and simulated spectra show good agreement. The transmission spectra of the Au monomers and ring-like quadrumers plotted in Figs. 2(a) and (b) reveal the excitation of dipolar mode, with a symmetric Lorentzian profile. As can be seen, the transmission dip of the ring-like quadrumer spectrum is deeper than that of the monomer spectrum due to the existence of more nano-disks on the substrate. From the transmission spectra, it can also be observed that the ring-like quadrumer structure behaves similarly to the isolated monomer due to the well-separated configuration of

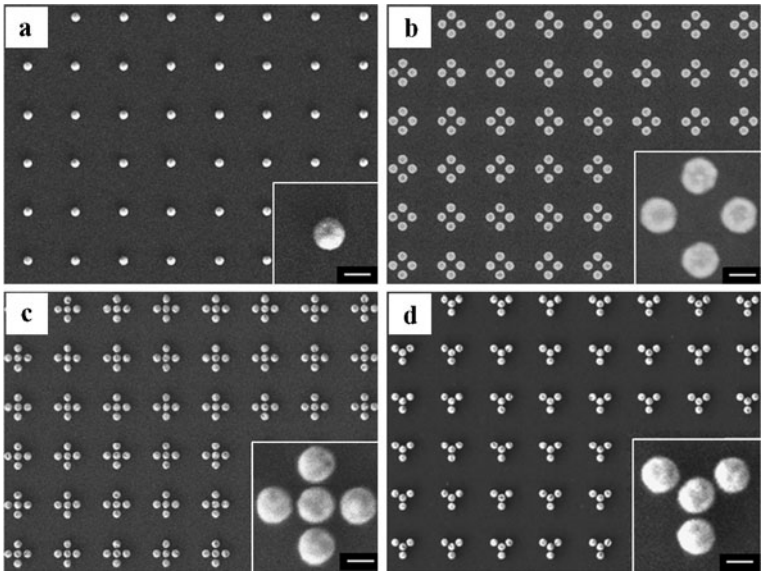

Fig. 1 SEM images of periodic array patterns of (**a**) monomers, (**b**) ring-like quadrumers, (**c**) pentamers and (**d**) quadrumers. Scale bar is 100 nm

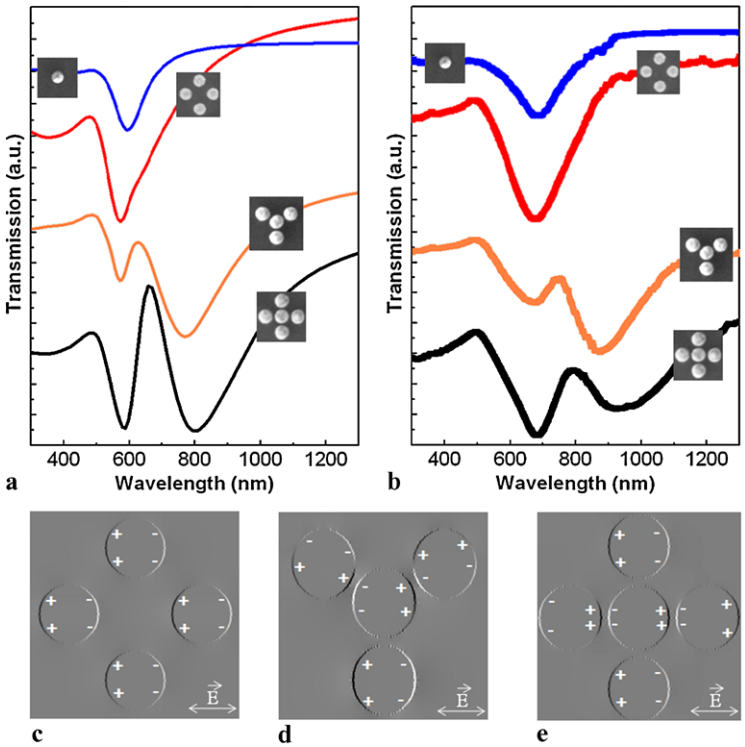

Fig. 2 (**a**) Simulated and (**b**) experimental transmission spectra of monomers, ring-like quadrumers, quadrumers and pentamers at x-polarized normal incidence. Calculated charge distribution for the (**c**) ring-like quadrumer at 650 nm, (**d**) quadrumer at 640 nm and (**e**) pentamer at a wavelength of 665 nm

the nano-disks. It can be determined from the orientation of charge distributions in the ring-like quadrumer after the resonance as shown in Fig. 2(c) around the wavelengths of 650 nm. This charge distribution displays that the plasmons in all four disks oscillate in phase, leading to the excitation of a broad super-radiant bright mode centered around 575 nm. It is worth mentioning that generally in the planar oligomers, the super-radiant bright mode comes to existence when the plasmons of all the nano-disks or particles oscillate in phase. The signature of the sub-radiant mode becomes apparent when the opposite anti-parallel dipolar moments appear [2, 12], leading to a reduction in the net dipole moment and hence a diminished coupling to incident light.

While the fabricated quadrumers in this work generate only a polarization-independent broad dipole resonance be-

cause of its high degree of symmetry [21], a unique spectral feature appears when a central nano-disk is introduced into the center of the ring-like quadrumer to form pentamer structure. In this case, the dipolar plasmon, arising from the central disk, hybridizes with the ring-like quadrumer dipolar plasmons, allowing the formation of a dark sub-radiant collective mode in addition to the bright super-radiant collective mode [22]. In the pentamers, it is obtained while the optical properties are kept polarization-independent due to the in-plane isotropic nature of the pentamer. The charge distribution pattern in a single pentamer at a wavelength of 665 nm is plotted in Fig. 2(e). It shows the configuration of anti-parallel modes where three middle disks oscillate in the opposite phase with respect to upside and downside disks. The effect of the anti-parallel dipolar modes in the pentamers leads to the formation of the sub-radiant mode. It can be observed from the transmission spectra in an asymmetric line-shape known as FR around 665 nm in Fig. 2(a) and around 770 nm in Fig. 2(b). The existence of FR in the pentamers demonstrates that the condition of the destructive interference between the sub-radiant mode and the super-radiant mode is sufficiently fulfilled. Meanwhile, the FR can also be observed in the transmission spectrum corresponding to the fabricated quadrumer. Figure 2(d) plots the calculated charge distribution pattern in a single quadrumer at a wavelength of 640 nm. It corresponds to the peak position in which the dark mode can be observed in the simulated transmission spectra for the quadrumers. The configuration of the anti-parallel dipole, which is responsible for the emergence of the sub-radiant mode can also be seen in this plot clearly. Though the upper disks exhibit a rotated charge distribution pattern with respect to the central nano-disk, the net sum oscillation directions of these two nano-disks are parallel to the oscillation direction of the downside nano-disk. In other words, at this wavelength the dipole moments of the central nano-disk oscillate totally out of phase.

Since the central nano-disk substantially dictates the transition from the isolated to the collective modes and plays a crucial role for the formation of the FR [2], it can be concluded that such kinds of design have the ability to switch on and off the FR in totally symmetric conditions either by adding or removing the central nano-disk. Heptamers, another planar symmetric structure in which FR can be exhibited, have the same possibility as well [2, 12]. But it is noticeable that in the heptamers, the destructive interference between the super-radiant and the sub-radiant modes happens when the net sum of the plasmons of the six outer disks oscillates oppositely with respect to the plasmon arising from the central nano-disk [2, 12]. Since the formation of the distinct Fano-like shape in the spectrum is due to this destructive interference, the contrast of the FR in the heptamers is lower than the FR investigated in this paper for both the quadrumers and pentamers. In this work, it is found that when the number of the outer disks is reduced, the ratio value between two collective opposite modes increases. It is a result of changing of the ratio between the opposing phase oscillating plasmons from $1/6$ in the heptamers to $1/3$ in the quadrumers and $2/3$ in the pentamers as shown in Figs. 2(d) and (e), respectively. The FRs corresponding to the quadrumers and pentamers can be observed clearly in the experimental spectra of Fig. 2(b) because of the rise in the FR contrast. It can promote the efficiency of biological and chemical detection [3].

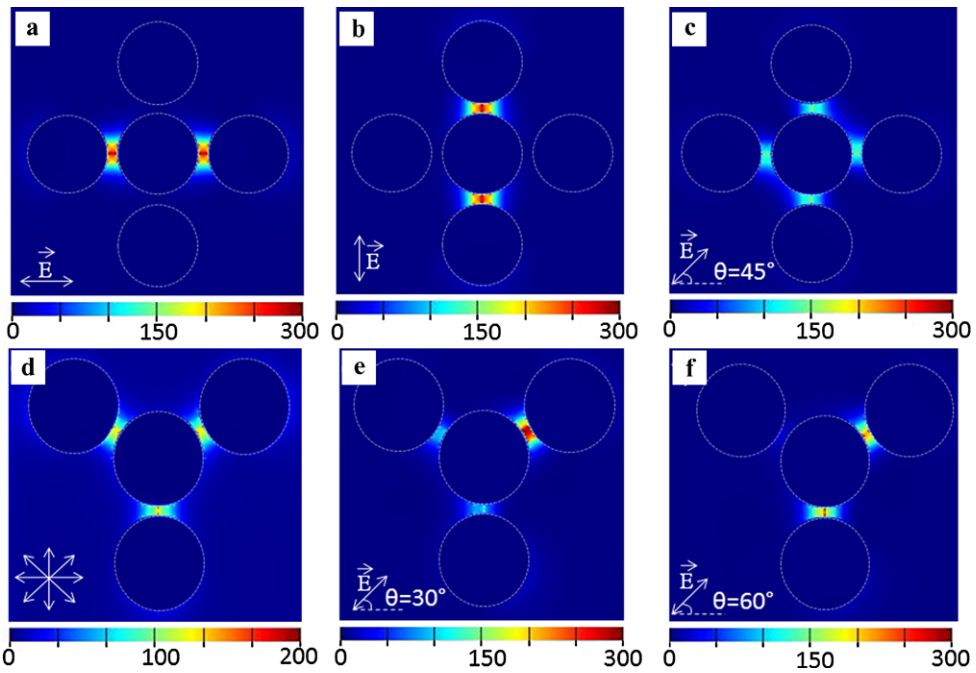

Fig. 3 Calculated near-field distribution of the pentamer at the wavelengths of 805 nm at (**a**) x-polarized, (**b**) y-polarized and (**c**) 45-degree polarized and the quadrumer at the wavelength of 780 nm at (**d**) non-polarized, (**e**) 30-degree polarized and (**c**) 60-degree polarized to normal light incidence

Figure 3 shows another interesting property of the pentamers and quadrumers. The linear-field distribution plots in this figure reveal that the near-field energy localization can achieve several hundred-fold intensity enhancement within the gaps among the three central nano-disk and the surrounding nano-disks of the pentamers and quadrumers. Figure 3(a) shows how the pentamer is able to concentrate light down to sub-20 nm gaps at the wavelength of 805 nm. It is the wavelength in which the effect of the destructive interference vanishes and the transmission spectrum resumes its constructive interference while all disks oscillate in phase again. This plot displays the local field intensity redistribution within the gaps among three middle disks at x-polarized illumination. The field intensity is enhanced significantly only inside the gaps. It reveals that these separated disks can be used as an optical antenna. Meanwhile, Figs. 3(b) and (c) show the pentamer structures at y-polarized and 45 degree-polarization (in X–Y plane) illumination, respectively. These plots demonstrate that the field can be strongly localized in the left and right gaps under x-polarized excitation, but in the top and bottom gaps under y-polarized excitation and in these four gaps under a 45-degree polarization. It is the unique feature of the pentamers to store light energy in different positions selectively by changing the polarization. We should keep in mind that the total amount of re-distributed field intensities, which are shown in Fig. 2, is kept constant during changing the polarization orientation. For spatial control over the nanoscopic field distribution, this structure does not require co-illumination by two light sources [17] and the adjustment of the phase delay between them [7, 17]. This advantage benefits potential applications for plasmon-based all optical information processing [17] and control of light matter interactions in the nanoscales [16, 23]. This ability can also be seen in the quadrumers at a wavelength of 780 nm. Figures 3(d)–(f) plot the spatial energy distributions with non-polarized incident light, 30° and 60° excitation polarization with respect to the x-axis, respectively. The unequal nanoscale triangular localized energies shown in Fig. 3(e) can overcome the difficulties of sharp corner exposure in plasmon-lithography [19]. Meanwhile, the energy localization pattern plotted in Fig. 3(e) shows how the quadrumer can be used as a planar optical switch [24] along the three directions simultaneously. As can be seen, when a 60° excitation polarization is applied, the near-field energy is localized at two gaps out of the three gaps inside the structure. The third gap exhibits almost no near-field energy. This unique ability to localize the near-field energy in the selected gaps between the nano-disks via the excitation polarization in quadrumers and pentamers provides the possibility to realize synchronized control systems in molecular nanoscale circuits [25].

Though the effect of nano-disk size and the gap among them on the optical properties of oligomers have been recently studied [2, 12, 26], a comprehensive study of this effect on "hot-spots" energies among the components of oligomers is not considered. In this work, the influence of the nano-disk dimension and the gap among them on the intensity and distribution shape of the localized near-field energy in pentamers and quadrumers is studied. For this purpose, the sizes of all components are taken as a constant. Table 1 in Fig. 4 lists the dimensions and sizes of six different sets of pentamers. Since the change in sizes and gap affects the optical properties, transmission spectra of each set are simulated and shown in Fig. 4(a). It helps to determine the wavelength in which the destructive interference vanishes and the structure resumes to exhibit plasmons constructively. Generally in the pentamers, the position of the second dip of transmission is the wavelength in which the pentamer exhibits the highest constructive intensity [13]. Consequently linear and logarithm scales of field distribution for each set of pentamers are calculated and shown in Figs. 4(b) and (c), respectively. The vertical bars indicate the color scale for the magnitude of the electric field intensity. The linear scale of the field distribution patterns can be used to show field intensity and the logarithm scale is useful to determine the direction of the electric field. Figure 4 reveals that the gap size among the disks plays a more important role than the disk size in terms of both intensity of Fano-like shape spectra and field intensity. As can be seen, the pentamers Types I and V at a the gap of 50 nm possess 80 and 70 times electric field enhancement, respectively, which are very close to each other. These two pentamers exhibit similar asymmetric Fano-shape spectra as well. The similar trend can be seen in the pentamers Types II and VI, in which, though the disk sizes are different, their optical properties are similar. The gap among the disks in these two pentamers is 30 nm. The calculated optical properties for the pentamer Type IV also support this conclusion that when the gap increases, both the electric field and FR intensities decrease. Finally the results of the pentamer Type III show that both the FR and electric field intensity increase significantly when the gap among the nano-disks is decreased to 10 nm. But the logarithm scale of electric field intensity of the pentamer Type III shows that this structure is not good enough anymore for the applications based on localization of "hot-spots" energy. In order to use an oligomer design for optical switching, non-linear spectroscopy and "hot-spots" energy, the energy localization plays very important role. In particular, one thinks of the field intensity distribution in the gaps among the nano-disks. It controls connection and disconnection among the metallic disks and promises extensive applications. As can be seen in logarithm scale we have the electric field distribution of pentamers Type III, and in the gaps which are allocated among the central disk and two disks located at upside and downside, the observed dark area is very small. It is the area in which the electric field possesses opposite direction. That is why upon to the polarization excitation along the x direction, the chance for interaction among

Table.1

	I	II	III	IV	V	VI
A	130	130	130	110	110	110
B	180	160	140	180	160	140
C	180	160	140	180	160	140

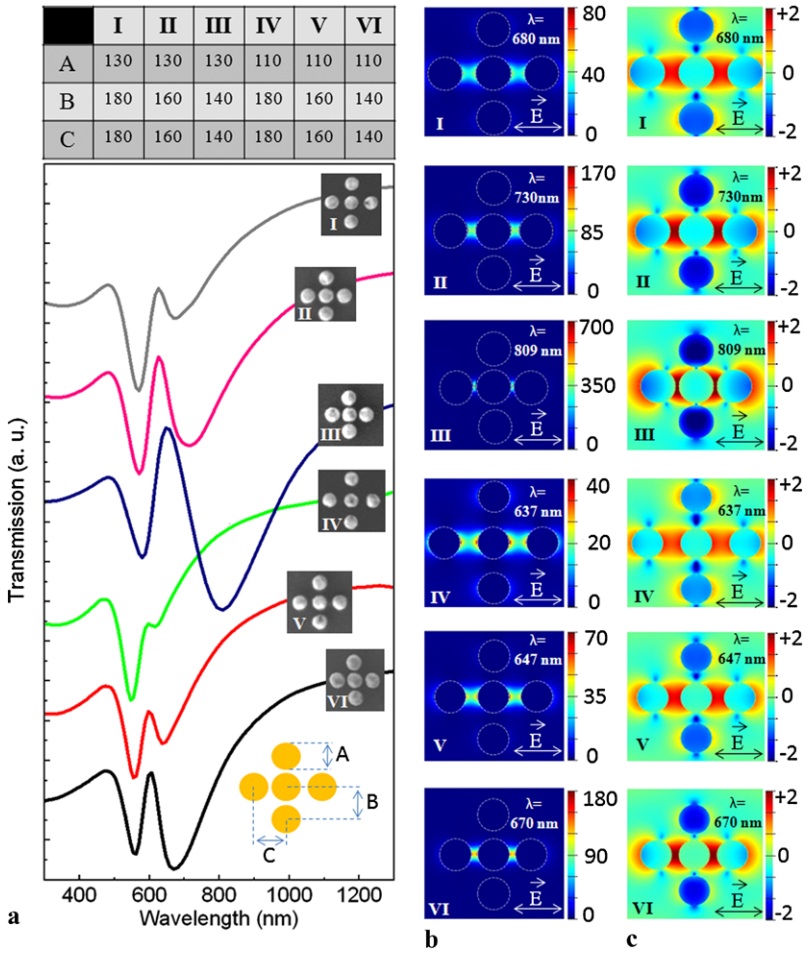

Fig. 4 *Table 1*: Dimensions of six various types of pentamer under consideration. (**a**) Simulated transmission spectra of six various types of pentamer at x-polarized normal incidence. (**b**) Linear and (**c**) logarithm calculated electric field distribution within the 6 various pentamer types at x-polarized normal incidence at the wavelength of the second deep in corresponding transmission spectra in (**a**)

plasmons arisen from vertical disks is much higher as compared to the other types of pentamer which possess bigger gap. On the other hand, the pentamers Types I, IV and V are good enough from this point of view, but the weak FR and low linear-field intensity of them make them unreliable for practical applications. Consequently the pentamer Type II with 30 nm gap among the disks is more suitable as an optical device with reliable FR intensity and tunable "hot-spot" localization.

Finally the effect of nano-disk sizes and the gaps among them on "hot-spots" among the components of quadrumers are studied. Table 2 in Fig. 5 shows the dimensions of four different sets of quadrumers. Simulated transmission spectra, and linear and logarithm scales of the electric field distribution for each set, are plotted in Figs. 5(a) to (c). Interestingly, when the gaps among nano-disks are reduced to 10 nm in the quadrumer Type II, the electric field intensity does not grow as much as the pentamer Type III at similar gaps. Here, the effect of the number of surrounding disks can be seen clearly. However, when the number of the surrounding disks is higher than four, the localization control of "hot-spots" is much more difficult because of the close distance among the surrounding disks. The similar optical properties between the quadrumers Types I and IV is also obvious, while the disk sizes are different and only the gaps among the disks are similar at 30 nm. However, the logarithm scale plots in Fig. 5(c) show that the quadrumer Type I is more reliable for practical applications due to better potential of electric field distribution control between central disk and downside disk. It promises extensive applications in contactless optical switches and non-linear spectroscopy. It is worth mentioning that the comparison among the near-field energies in this section for both the pentamers and quadrumers is established only among a few different sets and based on the results presented, further studies are required to explore the optimized oligomers.

4 Conclusions

In summary, the plasmonic quadrumer and pentamer exhibiting a pronounced contrast FR are investigated. The FR can be obtained under normal-incident light along all orientations of polarization. It is demonstrated that the monomers

Table.2

	I	II	III	IV
A	130	130	110	110
B	160	140	160	140
C	160	140	160	140

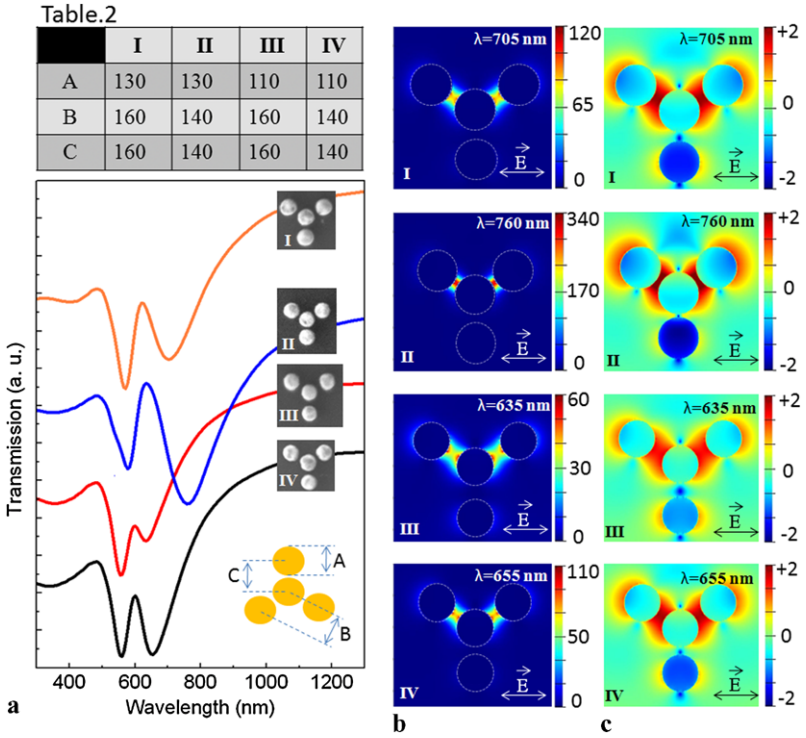

Fig. 5 *Table 2*: Dimensions of four different designs of the quadrumers. (**a**) Simulated transmission spectra of four different types of quadrumer at x-polarized normal incidence. (**b**) Linear and (**c**) logarithm scale of the calculated electric field distribution within the four various quadrumers at x-polarized normal incidence at the wavelength of the second deep in the corresponding transmission spectra of (**a**)

and ring-like quadrumers behave the same as the isolated nano-disks exhibiting only the isolated mode. After the addition of the central disk into the center of the ring-like quadrumers to form the pentamers, an anti-parallel coupling of dipolar modes appears. The ratio between the anti-parallel and parallel dipole modes is 2/3 and results in the generation of a pronounced FR as compared to the other planar symmetric structures. This trend can also be seen in plasmonic quadrumers at a ratio of 1/3 between anti-parallel and parallel dipole modes. Furthermore, it is shown that the quadrumer and pentamer can manipulate the localization of near-field energy distribution in a sub-diffraction length scale and overcome the spatial restrictions of conventional optics. The tuning of the spatial distribution of the light can be achieved by only a single source, instead of applying a phase shift in a co-illumination system. Finally, the influence of the nano-disks sizes and the gaps among them on the intensity and shape of the localized near-field energy distribution among different designs of the pentamers and quadrumers was studied.

Acknowledgements The authors would like to acknowledge the funding provided by SERC Agency of Science, Technology And Research (A*STAR) Superlens Program (Project No. 092 154 0099) for the research work published in this paper. Mohsen Rahmani would like to express his gratitude for the support from the A*STAR–SINGA program.

References

1. W.L. Barnes, A. Dereux, T.W. Ebbesen, Nature **424**, 824 (2003)
2. M. Hentschel, M. Saliba, R. Vogelgesang, H. Giessen, A.P. Alivisatos, N. Liu, Nano Lett. **10**, 2721 (2010)
3. B. Luk'Yanchuk, N.I. Zheludev, S.A. Maier, N.J. Halas, P. Nordlander, H. Giessen, C.T. Chong, Nat. Mater. **9**, 707 (2010)
4. K. Bao, N.A. Mirin, P. Nordlander, Appl. Phys. A, Mater. Sci. Process. **100**, 333 (2010)
5. N. Liu, L. Langguth, T. Weiss, J. Kästel, M. Fleischhauer, T. Pfau, H. Giessen, Nat. Mater. **8**, 758 (2009)
6. V. Giannini, Y. Francescato, H. Amrania, C.C. Phillips, S.A. Maier, Nano Lett. **11**, 2835 (2011)
7. C.L. Garrido Alzar, M.A.G. Martinez, P. Nussenzveig, Am. J. Phys. **70**, 37 (2002)
8. Y.S. Joe, A.M. Satanin, C.S. Kim, Phys. Scr. **74**, 259 (2006)
9. J. Ye, L. Lagae, G. Maes, G. Borghs, P. Van Dorpe, Opt. Express **17**, 23765 (2009)
10. M. Wickenhauser, J. Burgdörfer, F. Krausz, M. Drescher, Phys. Rev. Lett. **94**, 023002 (2005)
11. F. Hao, P. Nordlander, Y. Sonnefraud, P. Van Dorpe, S.A. Maier, ACS Nano **3**, 643 (2009)
12. J.B. Lassiter, H. Sobhani, J.A. Fan, J. Kundu, F. Capasso, P. Nordlander, N.J. Halas, Nano Lett. **10**, 3184 (2010)
13. M. Rahmani, B. Lukiyanchuk, B. Ng, A.K.G. Tavakkoli, Y.F. Liew, M.H. Hong, Opt. Express **19**, 4949 (2011)
14. M. Rahmani, B. Lukiyanchuk, T.T.V. Nguyen, T. Tahmasebi, Y. Lin, T.Y.F. Liew, M.H. Hong, Opt. Mater. Express **1**, 1409 (2011)
15. M. Rahmani, T. Tahmasebi, Y. Lin, B. Lukiyanchuk, T.Y.F. Liew, M.H. Hong, Nanotechnology **22**, 245204 (2011)
16. V. Giannini, A.I. Fernández-Domínguez, Y. Sonnefraud, T. Roschuk, R. Fernández-García, S.A. Maier, Small **22**, 2498 (2010)
17. X.R. Su, Z.S. Zhang, L.H. Zhang, Q.Q. Li, C.C. Chen, Z.J. Yang, Q.Q. Wang, Appl. Phys. Lett. **96**, 043113 (2010)
18. M. Aeschlimann, M. Bauer, D. Bayer, T. Brixner, F.J. García De Abajo, W. Pfeiffer, M. Rohmer, C. Spindler, F. Steeb, Nature **446**, 301 (2007)

19. W. Srituravanich, N. Fang, C. Sun, S. Durant, M. Ambati, X. Zhang, in *3rd Conf. Integrated Nanosystems*, Pasadena, CA, Sept. 2004. doi:10.1115/NANO2004-46023
20. P.B. Johnson, R.W. Christy, Phys. Rev. B **6**, 4370 (1972)
21. D.W. Brandl, N.A. Mirin, P. Nordlander, J. Phys. Chem. B **110**, 12302 (2006)
22. A. Christ, O.J.F. Martin, Y. Ekinci, N.A. Gippius, S.G. Tikhodeev, Nano Lett. **8**, 2171 (2008)
23. S.A. Maier, Nat. Mater. **8**, 699 (2009)
24. G. Margheri, T. Del Rosso, S. Sottini, S. Trigari, E. Egiorgetti, Opt. Express **16**, 9869 (2008)
25. M.A. Reed, T. Lee, *Molecular Nanoelectronics* (American Scientific Publishers, New York, 2003)
26. M. Hentschel, D. Dregely, R. Vogelgesang, H. Giessen, N. Liu, ACS Nano **5**, 2042 (2011)